Cross-helix separation of tropomyosin molecules in acto-tropomyosin as determined by neutron scattering

D. B. Bivin,* D. B. Stone,‡ D.K. Schneider,§ and R. A. Mendelson‖

*‖Cardiovascular Research Institute and ‡Department of Biochemistry and Biophysics, University of California, San Francisco, California 94143; and §Biology Division, Brookhaven National Laboratory, Upton, New York 11973 USA

ABSTRACT The cross-helix separation of Tm molecules in acto-tropomyosin has been determined using neutron scattering. Deuterated *Dictyostelium discoideum* actin was density matched in a 93% D_2O buffer so that effectively only the protonated tropomyosin was "visible" to neutrons. Analysis of the solution scattering pattern in the region of the first oscillation yielded a value for the cross-helix separation of 7.9 ± 0.3 nm. The implications of this value for the mechanism of the regulation of muscle contraction are discussed in light of recent results by others.

INTRODUCTION

In vertebrate muscle the regulation of force generation is brought about by the binding and unbinding of Ca^{2+} to the thin-filament based protein troponin. The binding of Ca^{2+} induces changes in the thin filament which result in the development of tension. In one view (Huxley, 1972; Parry and Squire, 1973), Ca^{2+} binding to troponin causes a change in the circumferential and radial position of the coiled-coil protein tropomyosin (Tm), which approximately follows the long-pitch actin groove. This change allows the myosin head access to an actin interaction site which had heretofore been sterically blocked by Tm. Recently, a somewhat different view has been proposed (Phillips et al., 1986). Regulation is thought to occur by changes in the (statistical) population of occupied Tm-binding sites on actin and by possible concomitant changes in thin-filament flexibility. In this view there is little change in the average radial position of Tm upon Ca^{2+} addition, and therefore the average cross-helix spacing between Tm molecules, d, is also constant. In either view d must be known to understand the mechanism of muscle regulation.

Because of the relatively small linear mass density of Tm compared with F-actin, it has not been possible to unambiguously define its position in reconstituted thin filaments by electron microscopy or by conventional diffraction methods. There is disagreement on even the value of d in one physiological state (See Milligan and Flicker, 1987; Popp et al., 1989).

We have initiated a program using neutron scattering with the aim of ultimately understanding the mechanism of vertebrate muscle regulation. In this method, the observed neutron intensity and diffraction is, to a good approximation, proportional to the square of the "contrast":

$$I(s) \propto (\bar{\rho}_{\text{protein}} - \rho_{\text{solvent}})^2, \quad (1)$$

where $\bar{\rho}_{\text{protein}}$ and ρ_{solvent} are the average scattering length densities of the protein and solvent, respectively. These densities, which are properties of atomic nuclei, can be varied over a wide range by replacing some or all of the ^1H by ^2H in the protein and/or solvent. Thus, it is possible to match out a protein matrix having a particular $\bar{\rho}_{\text{protein}}$ and observe the diffraction generated solely by one (or more) unmatched particle. Thus, the above-mentioned ambiguities in assignment of density can be eliminated in the study of many biological systems.

In this work we present a measurement of d for Tm bound to deuterated actin (Stone et al., 1987; Curmi et al., 1988.) Here, the scattering length density of deuterated actin was matched by a 93% D_2O solvent to render it effectively "invisible" in neutron scattering so that only neutron scattering by Tm, in the acto-Tm complex, is observed. Because Tm significantly inhibits acto-S1 ATPase at low S1 concentration, the acto-Tm system can serve as a model for the Tm position in thin filaments in the resting state (low Ca^{2+}) of intact muscle.

MATERIALS AND METHODS

Proteins

Deuterated *Dictyostelium discoideum* cells were grown on autoclaved deuterated *Escherichia coli*, as described by Stone et al. (1987). The process of purification of deuterated actin was modified by eliminating the use of a large gel filtration column as the first chromatographic step and, instead, proceeding directly to ion exchange chromatography (Gordon et al., 1976; Carboni and Condeelis, 1985). In addition to a

Dr. Bivin's present address is Dept. of Physiology, Univ. of the Pacific, San Francisco, CA 94115.

Address correspondence to Dr. Mendelson.

0006-3495/91/04/880/09 $2.00

more rapid purification of deuterated actin, this modification allowed us to easily increase the size of the preparation with little or no diminution in final purity or yield.

After cell lysis in a buffer containing 10 mM TEOLA (pH 7.5), 1 mM DTT and protease inhibitor cocktail (Stone et al., 1987) and subsequent centrifugation, the supernatant was applied to a Whatman DE-52 column. For a 10 l culture (70–100 g of cells), a 5 × 20 cm column, equilibrated with 10 mM TEOLA (pH7.5), 0.5 mM MgATP, 100 mM KCl, 0.1 mM $CaCl_2$, 1 mM DTT, was employed. Just before lysate addition, 50 ml of column buffer (without KCl) was applied to the column to allow penetration of actin without polymerization. After loading, the column was washed with 2 l of the column buffer with 0.12 M KCl present. A 1,500 ml gradient (0.12–0.6 M KCl) was run to elute actin. Actin-containing fractions were then further purified by ammonium sulfate fractionation, centrifugation, and gel filtration, as described previously (Stone et al., 1987).

Tropomyosin was isolated from rabbit skeletal muscle acetone powder and purified by hydroxylapatite chromatography (Eisenberg and Kielley, 1974).

Preparation of samples

Samples for neutron scattering were prepared on-site from freeze-dried G-actin and Tm. Rabbit skeletal Tm was freeze dried in a buffer consisting of 2 mM imidazole (pH 7) and 0.5 mM DTT at a concentration of 4 mg/ml. Deuterated actin was freeze dried at a concentration of 3 mg/ml in G-actin buffer consisting of 2 mM-imidazole (pH7.0), 0.1 mM-ATP, 50 μM-$CaCl_2$, 0.1 mM-DTT, 1 mM NaN_3, 1 ml/l protease inhibitor cocktail.

Freeze-dried actin was resuspended in 93% D_2O G-actin buffer (pD7.0) to a concentration significantly higher than the required final concentration. For example, for final 20 mg/ml and 40 mg/ml actin concentrations, pre-weighed actin was resuspended to known concentrations in the ranges of 30–40 mg/ml and 50–60 mg/ml, respectively. Pre-weighed Tm was resuspended to a known concentration in the range of 15–20 mg/ml in 93% D_2O containing 40 mM imidazole (pD7.0). Actin and Tm solutions were combined so that the final stoichiometry was 7:1 and 93% D_2O G-actin buffer was added to give a concentration slightly above the desired final concentration. Thorough mixing was achieved by drawing the solution into a Hamilton gas-tight syringe four or five times and then allowing the solution to stand for 1 h at 22°C.

Polymerization was initiated by adding concentrated KCl, $MgCl_2$, imidazole, and NaN_3 to achieve the desired actin concentration and the following buffer concentrations: 20 mM-imidazole (pD7.0), 80 mM-KCl, 0.1 mM-azide, 0.5 mM-DTT with the appropriate $MgCl_2$ concentration. After mixing and centrifugation at low speed in a desktop centrifuge to remove any air bubbles, the solution sat for 2 h at 22°C. It was then cooled to 6°C and loaded into cylindrical (6-mm diam × 4-mm thick) quartz sample cells.

Samples containing Tm and actin alone were prepared in a similar fashion. Buffer was substituted for protein, as appropriate.

Small-angle neutron scattering

Scattering patterns were obtained using the H9b beam line of Brookhaven National Laboratory's High Flux Beam Reactor (Schneider and Schoenborn, 1984). The wavelength (λ) used was 0.45 nm with a fractional spread $\Delta\lambda/\lambda = 0.12$ (full width at half maximum). The incident flux was typically 1–3 × 10^6 neutrons $s^{-1}cm^{-2}$. The sample-to-detector distance was 800 mm and the range of observed reciprocal space radius, s, was 0.045–0.8 nm^{-1}. ($s = 2 \sin [\theta]/\lambda$, where 2θ is the scattering angle.) An area detector (500 × 500 mm) with approximately 3.9 × 3.9 mm pixels was employed. The samples were maintained at 6°C, in 6 mm diam quartz cuvettes with 2- or 4-mm path lengths (depending on the H_2O/D_2O ratio in the solvent).

An automated sample holder (Engleman, 1979) was used to collect data cyclically from the samples: density-matched actin, Tm, acto-Tm, and a buffer. The exposure was determined by a (preset) beam monitor count. Typically the samples were exposed to the beam in succession for 20–30 min at a time. Total exposure times varied from 20 to 240 min.

The raw data consisted of two-dimensional arrays of neutron detector counts. The center of the array was found by exposing the detector to an attenuated direct beam. The mean distance of each pixel from the center of the beam was computed, and the average number of counts per pixel was determined as a function of s.

The scattering profiles were corrected for background (primarily buffer and ~10% residual scattering) using the following:

$$I_{net}(s) = I_{sample}(s) - k \cdot I_{back}(s), \quad (2)$$

where k was determined by summing the observed intensities for both the sample and the background between $s = 0.75$ and 0.80 nm^{-1} and then taking the ratio of the sums. In this region of the scattering curve, the scattering intensity contribution of the protein was small compared with that of the background ($I_{protein}:I_{back} < 1:1000$).

Extraction of structural parameters

Cross-sectional radius of gyration

At low-s the cross-sectional radius of gyration (R_x) was extracted from free Tm data by means of a cross-sectional Guinier plot of $s \cdot I(s)$ vs. s^2. Such plots were constructed from the low-s expression:

$$s \cdot I(s) = [s \cdot I(s)]_{s \to 0} \exp\{-2(\pi s R_x)^2\}. \quad (3)$$

Calculation of scattering functions

Scattering intensities were calculated from Tm model structures by filling models with closely packed spheres of uniform density (Mendelson and Kretzschmar, 1980) and then evaluating the Debye equation (1915) for the intensity as a function of s. These curves were smeared to mimic the nonideal neutron beam geometry and wavelength spread (Glatter, 1982).

Two models of the Tm molecule were used: one in which each Tm molecule consisted solely of a solid cylinder, and one consisting of two strands generated by solid coiled cylinders (Phillips et al., 1986) of variable pitch, strand radius, and in some cases, strand separation. In calculations involving Tm molecules bound to actin, Tm molecules were wrapped around the thin-filament axis (at variable d) with a full long-pitch repeat of 77 nm. Tm molecules on one side of the helix were shifted 2.75 nm axially with respect to their cross-helix partners.

Least-squares fitting to determine the cross-helix separation d[1]

To account for unpaired Tm (either free or bound to actin), it was assumed (see Results and Discussion) that the observed intensity arose from the sum of a paired and unpaired fraction:

$$I(s) = p \cdot I_{Tm\text{-}Tm}(s) + (1 - p) \cdot I_{Tm}(s). \quad (4)$$

[1]Because successive actin monomers are 167° apart rather than 180° and because cross-helix partner Tm molecules successively bind to these actin monomers, d will be equal to 1.9871 times the radial distance of the center of a Tm molecule from the helix axis rather than 2.0 times this distance.

Least squares fitting to extract d was accomplished as follows: a large number (125) of model curves ($I_{Tm\text{-}Tm}[s]$), were generated and stored. For differing values of p, slit and wavelength-smeared scattering curves were combined using Eq. 4, and the reduced χ^2's were computed over the s range of interest. Large ranges of p and all structural parameters were explored in uniform intervals to ensure that the search for a global minimum of χ^2 was exhaustive.

RESULTS

ATPase kinetics with deuterated actin

Previously, our laboratory reported a study of the acto-S1 ATPase with deuterated *Dictyostelium discoideum* actin (Curmi et al., 1988). Briefly, it was found that rabbit and both deuterated and protonated *Dictyostelium* actin behaved similarly in both H_2O and D_2O. The V_{max}'s were determined to be almost identical, while the K_{app}'s were about twice as large for both *Dictyostelium* actins as for rabbit actin.

To assess the ability of deuterated *Dictyostelium* actin to serve as a replacement for rabbit skeletal actin in studies of vertebrate muscle control, we have performed ATPase assays of reconstituted thin filaments under conditions approaching V_{max} (Walsh et al., 1984) using the method of Wagner and Weeds (1979).

Data in Table 1 indicate that both protonated and deuterated *Dictyostelium* actin, reconstituted with rabbit Tm and Tn, are indeed capable of regulating myosin-S1 ATPase in D_2O. A comparison of rabbit and *Dictyostelium* actin is shown in Table 2. Here it is seen that in addition to the ability to regulate ATPase to a comparable extent (with added Tm and Tn), both rabbit and *Dictyostelium* actin are inhibited by Tm-addition to a comparable extent. The similar behavior of all actins strongly indicates that the substitution of deuterated *Dictyostelium* actin for rabbit actin and the substitution of D_2O for H_2O does not alter the properties of thin-filament complexes.

TABLE 1 Effect of tropomyosin-troponin complex on the activation of myosin S-1 ATPase by protonated and deuterated *Dictyostelium* actin in D_2O

Additions	ACTO-S-1 ATPase (s^{-1})	
	0.2 mM EGTA	0.1 mM $CaCl_2$
33 μM ^{1}H-*Dictyostelium* actin	3.31	—
33 μM ^{1}H-*Dictyostelium* actin + 6.6 μM TM-TN	1.10	2.21
31 μM ^{2}H-*Dictyostelium* actin	4.14	—
31 μM ^{2}H-*Dictyostelium* actin + 6.3 μM TM-TN	1.66	3.59

ATPase assays were performed as described by Wagner and Weeds (1979) with a reaction volume of 100 μl containing 12 mM imidazole (pD 7.5, 25°C), 3 mM KCl, 1 mM DTT, 2 mM $MgCl_2$, 1 mM ATP, 0.05 μM chymotryptic subfragment 1 (obtained from rabbit skeletal muscle) in 97% D_2O.

TABLE 2 Effect of tropomyosin and troponin on the activation of subfragment 1 ATPase by rabbit skeletal and *Dictyostelium* actin

Additions	ACTO-S-1 ATPase (s^{-1})	
	0.2 mM EGTA	0.1 mM CaCl
29 μM rabbit skeletal actin	1.00	1.11
29 μM rabbit skeletal actin + 5.8 μM TM-TN	0.05 (5%)*	0.52 (47%)
29 μM rabbit skeletal actin + 5.8 μM TM	0.25 (25%)	0.30 (27%)
29 μM ^{1}H-*Dictyostelium* actin	0.78	0.68
29 μM ^{1}H-*Dictyostelium* actin + 5.8 μM TM-TN	0.05 (6%)	0.22 (32%)
29 μM ^{1}H-*Dictyostelium* actin + 5.8 μM TM	0.16 (21%)	0.13 (19%)

ATPase assays were performed as described by Wagner and Weeds (1979) with a reaction mixture containing 12 mM imidazole (pH 7, 20° C), 9 mM KCl, 5 mM $MgCl_2$, 2 mM ATP, 0.2 mM DTT, 1.24 μM chymotryptic subfragment 1 in H_2O. Skeletal actin, tropomyosin-troponin complex (TM-TN), and tropomyosin (TM) were prepared from rabbit back muscle. *Percent of actin-activated activity.

Scattering of neutrons by protonated tropomyosin

Neutron solution scattering by isolated Tm was investigated under the ionic conditions used in acto-Tm scattering experiments. The 93% D_2O buffer contained 80 mM-KCl, 2.5 mM-$MgCl_2$, 20 mM-Imidazole (pD7), 0.1 mM azide, 1 mM-DTT, and was maintained at 6°C. Under these conditions it is expected that some residual head-to-tail binding occurs (Asai, 1961; Tanaka and Oosawa, 1971) and indeed, we found that there is a measurable increase in the intrinsic viscosity compared with higher ionic strength conditions.

A Guinier plot of Tm data from a 9.2 mg/ml sample is shown in Fig. 1. Two phases may be seen in the plot. Below $s^2 \approx 0.02$ nm^{-2} there is a region which has a cross-sectional R_x near 0.9 nm, while the region $0.03 \leq s^2 \leq 0.15$ nm^{-2} yielded $R_x = 0.67 \pm 0.03$ nm. Here the stated error contains statistical error (small) as well as an estimate of systematic error, which arises primarily from error in buffer subtraction. Because of the difficulties arising from the high buffer scattering, we were unable to obtain satisfactory data much below 9 mg/ml. However, some data sets taken at 4 mg/ml showed qualitatively similar upsweeps at low-s^2, suggesting that

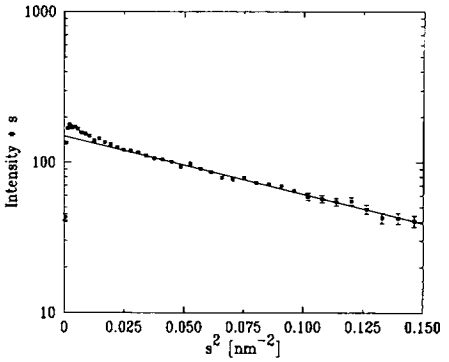

FIGURE 1 A cross-sectional Guinier plot of neutron scattering by free tropomyosin in a 93% D_2O buffer. The Tm concentration was 9 mg/ml. The solid line is from a linear least-squares fit over the range $0.03 \leq s^2 \leq 0.15$ nm^{-2}.

these upsweeps are not caused by equilibrium association. Determination of the s^2 intercept in these plots indicates that 85–90% of the mass/length has the lower value of R_x.

For simple models, calculations of R_x can readily be performed. If one takes 68,000 as the Tm molecular weight, 0.73 cm^3/g as the Tm partial specific volume, and 42.3 nm as the Tm length, a solid, cylindrical Tm has $R_x = 0.55$ nm. Variation of the molecular parameters within plausible ranges near these values does not signficantly alter R_x. If one assumes that, at low resolution, Tm resembles a pair of (*solid*) coiled cylinders which touch, but don't interpenetrate (Phillips et al., 1986), then $R_x = 0.685$ nm and the cylinder radius is $r = 0.558$ nm. The data are seen to be in good agreement with this value.[2] Here it was assumed that the cylinders coil around one another with a pitch of 13.7 nm, as suggested by the work of McLachlan and Stewart (1975) and Parry (1975); however, variation of the pitch over the range 12–15 nm does not significantly alter R_x. To determine if the super-coiling of Tm, as is found in the thin filaments and in Tm crystals (Phillips et al., 1986), could affect the measured R_x, we computed scattering curves for a single Tm coiled with a radius of 2.3 and 4 nm, to simulate crystal and thin filament super-coiling, respectively. Least-squares fits to these model curves over the two ranges showed no significant changes (< 0.2 nm) in the derived values for R_x in the range of the data in Fig. 1.

Thus, confirming Phillips et al. (1986), we find that coiled cylinders provide an adequate description of Tm at low resolution, whereas a simple solid cylinder does not. Although we cannot rule out all possible forms of Tm super-coiling, flexibility, and globular ends which could give the upsweep below $s^2 = 0.025$ nm^{-2} in Fig. 1, the simplest explanation for this upsweep is that some (10–15%) of the Tm forms aggregates and the rest resembles straight, or nearly straight, coiled cylinders in solution. This is also in agreement with rotary shadowing electron microscopy results (Flicker et al., 1982) which show that Tm in solution is extended and exhibits no apparent supercoiling.

Neutron scattering by Tm bound to Deuterated Actin

(I) Least-squares fitting of data

The expected diffraction and scattering by a pair of fully ordered coiled cylinders is shown in Fig. 2. Here it is seen that the low-s diffraction (Fig. 2 *b*) is dominated by the shallow helix-cross coming from the long repeat of Tm in the actin groove (Fig. 2 *a*). When the diffraction pattern is spherically averaged to simulate a solution experiment, the resultant scattering pattern (Fig. 2 *c*) exhibits oscillatory behavior with maxima near multiples of the reciprocal of d. This experiment is analogous to the Young's double slit Fraunhofer diffraction experiment of classical optics (with spherical averaging).

In the results to be described below, we have concentrated our analysis on data near the first oscillation. This oscillation arises primarily from the first layer line of the Tm diffraction pattern. We believe this prominent feature is least subject to experimental artifacts arising from residual scattering, aggregation, solution contaminants, and background subtraction errors. Also, as a very low-resolution feature, it is less subject to internal mass fluctuations of the scattering-length density-matched actin and to any disordering of TM on actin (e.g., Phillips et al., 1986) than are higher resolution features. The scattering intensities have been modeled by the sum of intensities arising from a fraction consisting of paired TM molecules bound to the actin and an unpaired fraction (see Methods). The unpaired intensity can arise from either single TM molecules bound to actin with no cross-helix neighbors, from unbound TM molecules free in solution, or from a combination of these two. Calculations comparing scattering by single TM molecules with varying degrees of super coiling, including TM bound in the actin groove, indicate that as long as the molecule is extended so that R_x is near the value measured above, there is no significant difference in scattering between

[2]Since we were unable to obtain a complete experimental concentration dependence of R_x(Tm), we cannot rule out inter-particle interference effects which would decrease the observed R_x. Thus, strictly speaking, the observed R_x is a lower limit on the true R_x. However, scattering by similar long rod-like proteins shows only small interparticle effects on R_x in the concentration range used here.

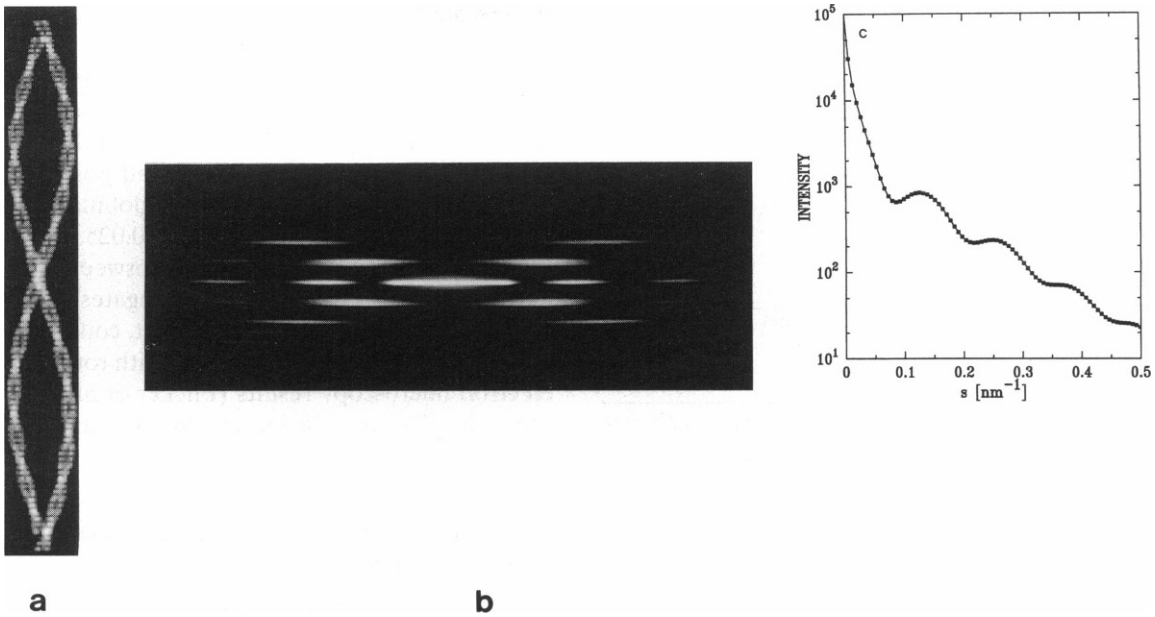

FIGURE 2 (*a*) Projected mass density of Tm pairs on actin. Here the strands of each Tm are coiled solid cylinders of radius 0.56 nm with a cross-helix spacing (*d*) of 7.9 nm. The full repeat of Tm is 77 nm. (*b*) The diffraction pattern generated by this model Tm. (*c*) The solution scattering pattern generated by this model. Calculations were performed using three full repeats (231 nm) of the model Tm show in *a*.

free and bound TM in the *s*-range of interest ($0.075 < s < 0.3$ nm^{-1}). Further, some modeling studies have been performed on paired Tm molecules with disorder. A Gaussian spread in *d* and *d* varying along the filament were considered. In the low-*s* range studied here, one cannot distinguish between these partially ordered situations and the paired-plus-unpaired (fully-ordered-plus-fully-disordered) model used here.

Acto-tropomyosin paracrystals

One concern we had from the beginning of these studies was that a small amount of residual acto-Tm paracrystal formation, which could conceivably occur even at low Mg^{2+} concentration, would distort our measurement of *d*. Inter-filament interference between Tm molecules might distort the *s*-region of interest since acto-Tm paracrystal spacings are known to be roughly comparable to the expected intra-filament Tm spacing. To investigate this possibility, we deliberately made (D)acto-Tm paracrystals and investigated their solution scattering under conditions where either actin or Tm alone was visible.

To set the contrast so that only actin in acto-Tm complexes was visible to neutrons, a buffer containing 41% D_2O was used. $MgCl_2$ was then added to form paracrystals. At 25 mM $MgCl_2$, significant turbidity appeared. At 50 mM $MgCl_2$, the turbidity was greater yet, though not obviously different from that at 100 mM $MgCl_2$. Also, samples with 25 mM $MgCl_2$ or greater were much more readily pelleted by centrifugation than were samples with less $MgCl_2$. The neutron scattering patterns (Fig. 3 *a*) were altered significantly, the effect much greater with 50 mM $MgCl_2$ than with 25 mM $MgCl_2$. Further, the strong shoulder near $s = 0.13$ nm^{-1} and the weak shoulder near $s = 0.2$ nm^{-1} were observed, as expected when paracrystals are formed. Fourier transforms of electron micrographs of acto-Tm paracrystals (Hanson et al., 1972) are heavily sampled on a row-line having a radial spacing of $\sim 1/7.5$ nm^{-1}. Sampling on the equator and on the 1/5.9 nm^{-1} layer-line generates the aforementioned shoulders in our solution scattering data. (A broad weak shelf seen in the no-$MgCl_2$ data between $s = 0.17$ and $s = 0.21$ nm^{-1} probably arises from the strong continuous actin layer-line with a meridional spacing of 1/5.9 nm^{-1}.)

The above results in 41% D_2O indicate that the deuterated actin + Tm behaves in a manner similar to protonated actin + Tm in H_2O: at 25 mM $MgCl_2$ some paracrystal formation occurs, and at 50 mM $MgCl_2$ paracrystals are well developed. Further, the packing of actin in acto-Tm paracrystals is readily sensed by neutron scattering. On the other hand, the acto-Tm complex in 93% D_2O (where the signal arises from Tm) showed only a small change with added $MgCl_2$ (Fig. 3 *b*). This change was almost identical at $MgCl_2$ concentrations of 25 and 50 mM even though the behavior of the turbidity

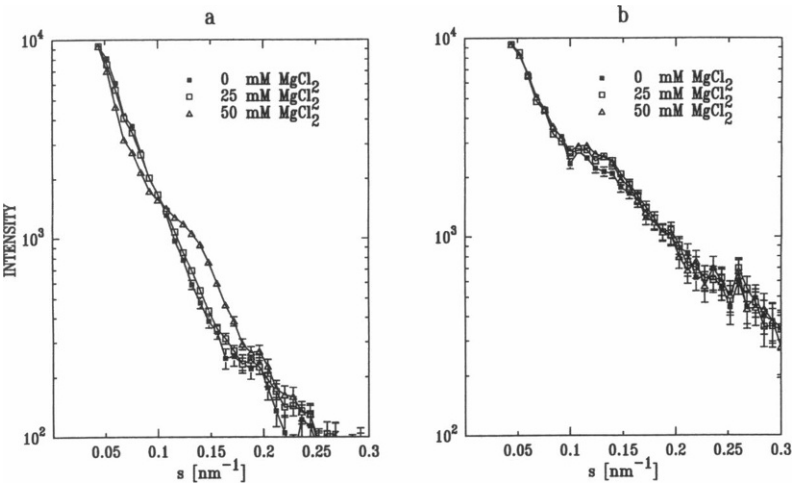

FIGURE 3 Acto-Tm paracrystal formation with varying concentrations of $MgCl_2$. (*a*) The buffer contains 41% D_2O so that only deuterated actin scattering is observed. Additionally, the acto-Tm (10 mg/ml actin) solution contained 20 mM-imidazole (p0.42D7.0), 80 mM-KCl, 0.5 mM-dithiothreitol, and 1 mM NaN_3 at 6°C. (*b*) The buffer contained 93% D_2O so that only Tm scattering is observed. Other conditions are identical except that the actin concentration is 20 mg/ml and pD7. Background subtraction was made on each sample (see Eq. 2). All scattering curves were normalized at $s = 0.044$ nm^{-1}.

and sedimentation was not noticeably different from acto-Tm in a 41% D_2O buffer. Separate experiments with $MgCl_2$ concentrations of 0, 2.5, 10, and 25 mM indicated (Fig. 4) that the change in the scattering patterns saturated between 2.5 and 10 mM of $MgCl_2$, far below where paracrystal formation is significant.

To quantify the effect of adding $MgCl_2$ in terms of a change in d, we have done a least-squares fit over the s-range from 0.068 to 0.244 nm^{-1} to the data shown in Fig. 4. The results are shown in Table 3. The variation in extracted d with increasing Mg^{2+} is found to be quite small, and as will be seen below, insignificant. It thus appears that any small amount of paracrystal formation that might be present at low Mg^{2+} concentrations will have an insignificant effect on the determination of the value of d. The Mg^{2+} dependence of the scattering patterns at added $MgCl_2$ concentrations below 10 mM appears to arise from a variation in Tm binding to actin and/or possibly changes in actin polymer length with increasing Mg^{2+}.

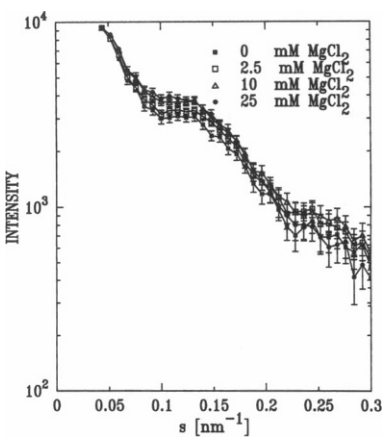

FIGURE 4 Change in scattering from Tm within acto-Tm complexes with varying $MgCl_2$ concentration. Sample conditions were the same as in Fig. 3 *b*. Background subtraction was made on each sample. Data were normalized at $s = 0.044$ nm^{-1}.

Neutron scattering Tm in acto-Tm filaments

Results of least-squares fitting at different acto-TM concentrations are summarized in Table 4. Initially, calculations were done with values of d ranging from 6.5 to 8.5 nm. It was found that, as expected from the position of the maxima of the fixed oscillation, only values near 8 nm gave reasonable fits ($\chi^2_\nu < 2$). The search range was then narrowed and a finer mesh of parameters was considered.

The results in Table 4 show no significant variation in

TABLE 3 Mg^{2+} Dependence of cross-helix separation

Mg^{2+}	p	d	χ^2_ν
mM		*nm*	
0.0	0.69	7.8	0.69
2.5	0.77	7.8	0.40
10.0	0.73	7.9	0.73
25.0	0.73	8.0	1.71

Data were fit over the interval $0.068 < s < 0.244$ nm^{-1}.

TABLE 4 **Results of least-squares fitting**

Fitted range of s	d	p	r	χ^2_ν
nm	*nm*		*nm*	
20 mg/ml actin				
$0.052 < s < 0.196$	7.9	0.72	0.57	0.38
$0.060 < s < 0.236$	7.8	0.77	0.62	0.40
$0.076 < s < 0.316$	7.8	0.76	0.62	0.33
30 mg/ml actin				
$0.052 < s < 0.196$	7.8	0.78	0.62	1.52
$0.060 < s < 0.236$	8.0	0.83	0.62	1.02
$0.076 < s < 0.316$	8.1	0.94	0.61	0.74
40 mg/ml actin				
$0.052 < s < 0.196$	7.9	0.73	0.59	1.70
$0.060 < s < 0.236$	7.8	0.73	0.62	1.06
$0.076 < s < 0.316$	7.8	0.69	0.61	1.76

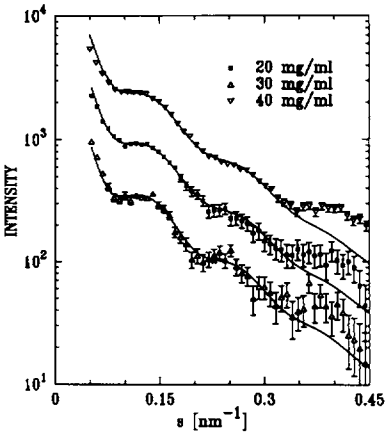

FIGURE 5 Least-squares fit to acto-Tm data in 93% D_2O. Data were fit over the range $0.06 < s < 0.234$ nm^{-1}. The solid curves are the fits using the parameters given in Table 4. Net counts are plotted for each concentration except the 40 mg/ml data were multiplied by two for display purposes. Data at each concentration were obtained on three different occasions using different deuterated actin preparations.

d with protein concentration. Also there are no significant differences in d for the different s-ranges used in the fits. Further, the value of d does not vary significantly with the fraction of Tm paired. Variation of the relative phase of the 13.7 nm repeat of one Tm with respect to its cross-helix partner Tm didn't significantly alter the goodness of fit or the extracted value of d.

The 30 mg/ml data are a result of a titration of Tm to increase the fraction of paired Tm molecules (p). This resulted in a significant increase in p. Sedimentation studies of binding showed that the bound fraction (b) of Tm was >0.90 in this sample, while other samples exhibited b values in the range of 0.80–0.90. We note that p need not equal b. For $b > 0.5$, the fraction paired can vary between $2b - 1$ and b depending on the propensity of Tm to have cross-helix neighbors.

We note that almost all fits (including data not shown) gave values for the strand radius of $r = 0.60$–0.63 nm. These values are larger than expected from the Tm solution scattering data which gave $r = 0.56 \pm 0.03$ nm. A source of some of this discrepancy may lie in the fact that the ends of Tm probably overlap by ~ 1.4 nm (Cohen et al., 1973; McLachlan and Stewart, 1975) when bound to actin. This overlap increases the filament-averaged strand radius slightly. It is also possible that the large r comes from systematic errors arising from background subtraction and/or the inadequacy of the coiled cylinder model of Tm. Slight variation in the amount of background subtracted was found to significantly alter p and r, but left d unaffected. Tm models with the strand separation increased by 0.1–0.2 nm beyond the "just touching" model considered above yielded lower χ^2_ν, decreased r, and increased p, but also left d unaltered.

We note that the fit to the data (Fig. 5) appears to extend up to about $s = 0.33$ nm^{-1}, where a feature which is not predicted by the model is seen. Although it is possible that this feature arises from a diffraction peak caused by Tm taking up the actin periodicity, such high resolution features must be interpreted with care. Fluctuations of the scattering length density of the matched actin could interfere with Tm and perhaps produce such artifacts (see Moore, 1981).

Based on results in Table 4, an assessment of absolute and possible systematic errors, we find that the value of d is 7.9 ± 0.3 nm. One source of systematic error that is difficult to assess is the effect of possible distortions arising from the above mentioned scattering-length density fluctuations of the contrast-matched actin. However, as shown in Fig. 5, the fit of the model curve to the data is good in the region considerably beyond that used in the least-squares fitting. Because distortions due to fluctuations in the matched scattering length density will increase with increasing s, this suggests that this phenomenon is negligible in the lower s region where the fitting was done.

SUMMARY AND DISCUSSION

In actin-tropomyosin complexes, a measurement of the mean cross-helix separation, d, of tropomyosin molecules has been made using neutron scattering. With deuterated actin matched out in 93% D_2O buffer, it was found that $d = 7.9 \pm 0.3$ nm. This value is in good agreement with electron microscopy of acto-Tm (O'Brien et al., 1983) and with a model based on tropomyosin

crystallography (Phillips, 1986), but does not agree well with a preliminary report of x-ray scattering measurements on acto-Tm complexes (Popp et al., 1989). In the latter study, a value of d = 6.95 nm was obtained by utilizing measured cross-sectional radii of gyration of actin and acto-Tm. We are unable to explain this discrepancy. However, neutron scattering measurements are able to directly sense Tm without significant background interference from actin, whereas actin scattering is dominant in x-ray experiments.

It is also interesting to note that the neutron experiments give nearly the same d value as found by electron microscopy of thin filaments decorated with S1 (Milligan and Flicker, 1987). In the latter work the presence of a high stoichiometry of S1 to actin is expected to put the thin filament in the "potentiated" state (see Murray et al., 1982) where the S1-ATPase (per head) exceeds that at very low stoichiometries. In the traditional steric blocking model, S1 (or Ca^{2+}) promotes movement of Tm away from the S1 binding site on actin to perhaps the position farthest from that in the "off" state. If such is the case, then one might expect to see a change in d between the off state and the "fully on" or potentiated state that is larger than that induced by Ca^{2+} addition alone. Because Tm inhibits acto-S1 ATPase when the S1 to actin ratio is low (Lehrer and Morris, 1982; Williams et al., 1988), we would expect that Tm in the experiment reported here would be closer to the off configuration than to the fully on state. The Ca^{2+} induced change in d is expected to be of the order of 0.5–2.5 nm based upon modeling studies of changes in the second layer line in intact muscle (see Parry and Squire, 1973; Huxley, 1972; Yagi and Matsubara, 1989). It would thus be expected that according to the traditional steric-blocking hypothesis the current experiments would yield a significantly different d value from that obtained from the S1 plus thin filament experiments. Alternately, Tm could move along a purely circumferential trajectory in response to S1 and/or Ca^{2+} and still regulate by a steric blocking mechanism. While the x-ray scattering experiments of Popp et al. (1989) indicate that significant differences in d do not occur in response to Ca^{2+}, further experiments are needed to decisively settle this issue.

The recent report (Kabsch et al., 1990) of the solution of the structure of monomeric actin at atomic resolution and a derived model for the F-actin structure (Holmes et al., 1990) indicates that it may soon be possible to position Tm in acto-Tm and perhaps ultimately in fully reconstituted thin filaments in more than one state. The present experiment indicates that neutron experiments with a fully regulated, reconstituted, thin filament are feasible. Such experiments will set the radial position of Tm in the thin filament and will allow a direct comparison of on and off states within one experimental system. We expect such experiments will aid in understanding the thin filament changes responsible for regulation.

The authors wish to thank Drs. P. Curmi, B. Schoenborn, M. Morales, and G. Phillips for helpful discussions at various stages of this work.

We gratefully acknowledge use of the University of California at San Francisco Computer Graphics Laboratory, which is supported by National Institutes of Health (N.I.H.) grant RR-1081. Dr. Bivin was a United States Public Health Service trainee (HL-07192). Supported by N.I.H. grant H1-16683 and National Science Foundation grant DMB-8716091.

Received for publication 17 August 1990 and in final form 16 November 1990.

REFERENCES

Asai, H. 1961. Electrical birefringence of rabbit tropomyosin. *J. Biochem.* 50:182–189.

Carboni, J. M., and J. S. Condeelis. 1985. Ligand-induced changes in the location of actin, myosin, 95K (α-Actinin), and 120K protein in amebae of *Dictyostelium discoideum*. *J. Cell Biol.* 100:1884–1893.

Cohen, C., D. L. D. Caspar, J. P. Johnson, K. Nauss, S. S. Margossian, and D. A. D. Parry. 1973. Tropomysoin-troponin assembly. *Cold Spring Harbor Symp. Quant. Biol.* 37:287–297.

Curmi, P. M. G., D. B. Stone, D. K. Schneider, J. A. Spudich, and R. A. Mendelson. 1988. Comparison of the structure of myosin subfragment 1 bound to actin and free in solution: a neutron scattering study using actin made "invisible" by deuteration. *J. Mol. Biol.* 203:781–798.

Debye, P. 1915. Zerstreuung von röntgenstrahlen. *Annu. Phys. (Leipzig).* 46:2927–2929.

Engleman, D. M. 1979. Neutron-scattering measurement of protein pair scattering functions from ribosomes containing deuterated proteins. *Methods Enzymol.* 59:656–669.

Eisenberg, E., and W. W. Kielley. 1974. Troponin-tropomyosin complex: column chromatographic separation and activity of the three active troponin components with and without tropomyosin present. *J. Biol. Chem.* 249:4742–4748.

Flicker, P. F., G. N. Phillips, Jr., and C. Cohen. 1982. Troponin and its interactions with tropomyosin. *J. Mol. Biol.* 162:495–501.

Glatter, O. 1982. Data treatment. *In* Small Angle X-ray Scattering. O. Glatter and O. Kratky, editors. Academic Press, London. 119–165.

Gordon, D., E. Eisenberg, and E. D. Korn. 1976. Characterization of cytoplasmic actin isolated from *Acanthamoeba castellanii* by a new method. *J. Biol. Chem.* 251:4778–4786.

Hanson, J., V. Lednev, E. J. O'Brien, and P. M. Bennett. 1972. Structure of the actin-containing filaments in vertebrate skeletal muscle. *Cold Spring Harbor Symp. Quant. Biol.* 37:311–318.

Holmes, K. C., D. Popp, W. Gebhard, and W. Kabsch. 1990. Atomic model of the actin filament. *Nature (Lond.).* 347:44–49.

Huxley, H. E. 1972. Structural changes in the actin- and myosin-containing filaments during contraction. *Cold Spring Harbor Symp. Quant. Biol.* 37:361–376.

Kabsch, W., H. G. Mannherz, D. Suck, E. F. Pai, and K. Holmes. 1990. Atomic structure of the actin:DNAse I complex. *Nature (Lond.).* 347:37–43.

Lehrer, S. S., and E. P. Morris. 1982. Dual effects of tropomyosin and troponin-tropomyosin on actomyosin subfragment 1 ATPase. *J. Biol. Chem.* 257:8073–8080.

McLachlan, A. D., and M. Stewart. 1975. Tropomyosin coiled-coil interactions: evidence for an unstaggered structure. *J. Mol. Biol.* 98:293–304.

Mendelson, R. A., and K. M. Kretzschmar. 1980. Structure of myosin subfragment 1 from low angle x-ray scattering. *Biochemistry.* 19:4103–4108.

Milligan, R. A., and P. F. Flicker, 1987. Structural relationships of actin, myosin, and tropomyosin revealed by cryo-electron microscopy. *J. Cell Biol.* 105:29–39.

Moore, P. B. 1981. On the estimation of the radius of gyration of the subunits of macromolecular aggregates of biological origin *in situ*. *J. Appl. Crystallogr.* 14:237–240.

Murray, J. M., M. K. Knox, C. E. Trueblood, and A. Weber. 1982. Potentiated state of the tropomyosin actin filament and nucleotide-containing myosin subfragment 1. *Biochemistry.* 82:906–915.

O'Brien, E. J., J. Couch, G. R. P. Johnson, and E. P. Morris. 1983. Structure of actin and the thin filament. *In* Actin—Its Structure and Function in Muscle and Non-Muscle Cells. J. Barden and C. dos Remedios, editors. Academic Press, Australia. 1–15.

Parry, D. A. D. 1975. Analysis of the primary sequence of α-tropomyosin from rabbit skeletal muscle. *J. Mol. Biol.* 98:519–535.

Parry, D. A. D., and J. M. Squire. 1973. Structural role of tropomyosin in muscle regulation: analysis of the x-ray diffraction patterns for relaxed and contracting muscle. *J. Mol. Biol.* 75:33–55.

Phillips, G. N. Jr., J. P. Fillers, and C. Cohen. 1986. Tropomyosin crystal and muscle regulation. *J. Mol. Biol.* 192:111–127.

Phillips, G. N. 1986. Construction of an atomic model for tropomyosin and implications for interactions with actin. *J. Mol. Biol.* 192:128–130.

Popp, D. M., Y, Maéda, and K. Holmes. 1989. X-ray evidence for four different conformations of the thin filament. *Biophys. J.* 55:201a. (Abstr.).

Schneider, D. K., and B. P. Schoenborn. 1984. A new neutron small-angle diffraction instrument at the Brookhaven high flux beam reactor. *In* Neutrons in Biology. B. P. Schoenborn, editor. Plenum Press, New York. 119–141.

Stone, D. B., P. M. G. Curmi, and R. A. Mendelson. 1987. Preparation of deuterated actin from *Dictyostelium discoideum*. *Methods Cell Biol.* 28:215–229.

Tanaka, H., and F. Oosawa. 1971. The effect of temperature on the interaction between F-actin and tropomyosin. *Biochim. Biophys. Acta.* 253:274–283.

Wagner, P., and A. G. Weeds. 1979. Determination of the association of mysosin subfragment 1 with actin in the presence of ATP. *Biochemistry.* 18:2260–2266.

Walsh, T. P., C. E. Trueblood, R. Evans, and A. Weber. 1984. Removal of tropomyosin overlap and the co-operative response to increasing calcium concentrations of the acto-subfragment-1 ATPase. *J. Mol. Biol.* 182:265–269.

Williams, D. L., Jr., L. E. Greene, and E. Eisenberg. 1988. Cooperative turning on of myosin subfragment 1 adenosinetriphosphatase activity by the troponin-tropomyosin-actin complex. *Biochemistry.* 27:6987–6993.

Yagi, N., and I. Matsubara. 1989. Structural changes in the thin filament during activation studied by x-ray diffraction of highly stretched skeletal muscle. *J. Mol. Biol.* 208:359–363.